

S-Wave Pseudoscalar-Meson-Baryon Scattering in a Simple Model with Broken $SU(3)$ Symmetry*

H. W. WYLD, JR.

Department of Physics, University of Illinois, Urbana, Illinois

(Received 15 August 1966)

A model of S -wave pseudoscalar-meson-baryon scattering is studied in which the force is due to vector-meson exchange. The potential is approximated by a static Yukawa potential and the kinematics is simplified. The actual physical masses of the particles are used so that $SU(3)$ symmetry is broken. The resulting problem reduces to a set of coupled-channel Schrödinger equations which are solved exactly on a computer. The K matrix and the eigenphases are calculated. Several examples of virtual bound-state resonances are found. The model yields a $Y_0^*(1405)$ as a virtual bound state of $\bar{K}N$ and an $N_{1/2}^*(1570)$ as a virtual bound state of $K\Sigma$.

I. INTRODUCTION

RECENT pion-nucleon phase-shift analyses¹⁻³ have uncovered an unexpectedly complex system of resonant and near-resonant states. In Fig. 1, for example, we give the Argand diagram for the S_{11} πN scattering amplitude as determined in Ref. 1 and 2. The curves are taken from Refs. 2 and 4. As we see from this figure the phase-shift determinations are still fraught with considerable uncertainty. There is, however, clear evidence for some sort of quasis resonant behavior, which we shall call $N_{1/2}^*(1570)$, slightly above the ηN threshold at 1490 MeV. This inelastic resonance has been the subject of several recent papers. Both Hendry and Moorhouse⁵ and Uchiyama-Campbell and Logan⁶ have carried out phenomenological analysis of the reaction $\pi^- p \rightarrow \eta n$ which indicate the presence of a resonance just above the ηN threshold. There is also some indication in Fig. 1 for a higher S_{11} πN resonance at about 1700 MeV.

Turning to the hypercharge zero states in the $l=0$ partial wave of the pseudoscalar-meson-baryon system we have the well-known $Y_0^*(1405)$ which, following Dalitz and Tuan, is thought to be an S -wave $\bar{K}N$ virtual bound state which decays through the coupled $\pi\Sigma$ channel.^{7,8} There is also a $Y_0^*(1670)$ associated with the $\eta\Lambda$ threshold in the same way as the $N_{1/2}^*(1570)$ is associated with the ηN threshold.⁹ There may also be a Y_1^* associated with the $\eta\Sigma$ threshold.¹⁰

* This work was supported by the National Science Foundation under Contract No. NSF GP 5622 and the U. S. Office of Naval Research under Contract No. 1834(05).

¹ P. Bareyre, C. Brickman, A. V. Stirling, and G. Villet, Phys. Letters **18**, 342 (1965).

² B. H. Bransden, P. J. O'Donnell, and R. G. Moorhouse, Phys. Rev. **139**, B1566 (1965).

³ A. Donnachie, A. T. Lea, and E. Lovelace, Phys. Letters **19**, 146 (1965).

⁴ R. H. Dalitz, in *Proceedings of the Oxford International Conference on Elementary Particles, 1965* (Rutherford High-Energy Laboratory, Harwell, England, 1966).

⁵ A. W. Hendry and R. G. Moorhouse, Phys. Letters **18**, 171 (1965).

⁶ F. Uchiyama-Campbell and R. K. Logan, Phys. Rev. **149**, 1220 (1966).

⁷ R. Dalitz and S. F. Tuan, Ann. Phys. (N.Y.) **10**, 307 (1960).

⁸ J. K. Kim, Phys. Rev. Letters **14**, 29 (1965).

⁹ D. Berley, P. F. Connolly, E. L. Hart, D. C. Rahm, D. L.

In addition to these resonances there is an $I=\frac{3}{2}$ resonance, $N_{3/2}^*(1670)$, which is clearly indicated in the phase-shift analysis of Ref. 1. The model discussed in this paper cannot account for this resonance.

We present in this paper a numerical study of a simple model of S -wave pseudoscalar-meson-baryon scattering in which the interaction is represented by a static-vector-meson-exchange potential. This model has been discussed extensively by Sakurai, who has shown that it leads to a qualitative explanation of some features of the S -wave πN , KN , and $\bar{K}N$ interactions.¹¹

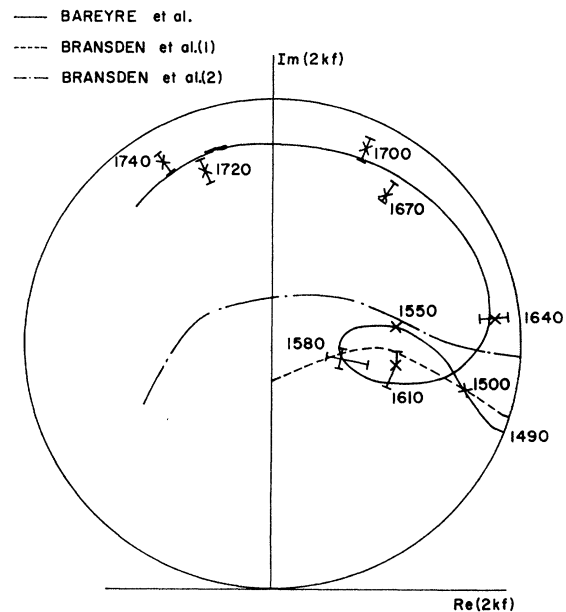


FIG. 1. The Argand diagram of the S_{11} - πN scattering amplitude. The numbers are energies in MeV. The curves are taken from Refs. 1, 2, and 4.

Stonehill, B. Thevenet, W. J. Willis, and S. S. Yamamoto, Phys. Rev. Letters **15**, 641 (1965).

¹⁰ D. B. Cline and M. G. Olsson, Bull. Am. Phys. Soc. **11**, 76 (1966).

¹¹ J. J. Sakurai, Ann. Phys. (N.Y.) **11**, 1 (1960); R. C. Arnold and J. J. Sakurai, Phys. Rev. **128**, 2808 (1962); J. J. Sakurai, in *Proceedings of the International School of Physics "Enrico Fermi" Course 26* (Academic Press Inc., New York, 1963), p. 41.

The potential in the model is a Yukawa potential. For such a potential it is a well-known result of elementary scattering theory that there are no S -wave resonances in a single-channel scattering problem. In order to obtain an S -wave resonance in a one-channel problem one would need a potential with a repulsive lip outside an attractive well. On the other hand, Fonda and Newton¹² and Dalitz and Tuan⁷ have shown that it is possible to obtain narrow S -wave resonances in multi-channel scattering problems. In this case the resonance is essentially a bound state in a higher-mass closed channel which decays through a coupled lower-mass open channel. Such resonances have been called virtual bound-state resonances by Dalitz. In order to obtain such resonances we need coupled channels with different masses. In the present calculation the coupled channels are obtained by using an $SU(3)$ version of Sakurai's vector-exchange model so that, for example, the πN , ηN , $K\Lambda$, and $K\Sigma$ channels are coupled together. In order to obtain different masses for the coupled channels we break the $SU(3)$ symmetry by using the actual masses of the various particles.

The calculations in this paper are based on the coupled-channel Schrödinger equation with a matrix potential. They are thus similar to those of Fonda and Newton¹² although the particular examples considered and the details of the calculation are quite different. The calculations are very much like those of Dalitz, Wong, and Rajasekaran,¹³ who concern themselves exclusively with the $Y_0^*(1405)$ resonance. Because there are relatively few examples in the literature of detailed numerical calculations for multichannel scattering problems, we have presented our results at some length. Even if the model should turn out to be wrong, the results of the calculation may be interesting as examples.

In detail the model used in this paper is the following: The force between the pseudoscalar-meson octet and the baryon octet is provided by the exchange of the vector-meson nonet as indicated in Fig. 2. At the BBV vertex we assume the $SU(3)$ -invariant interaction

$$i\sqrt{2}g_{pp\rho 0}[\bar{B}_j^k\gamma_\mu B_k^i - \bar{B}_k^i\gamma_\mu B_j^k]V_{\mu j}^i, \quad (1)$$

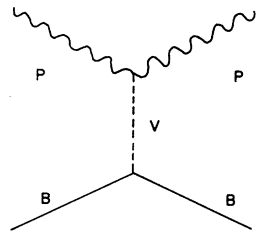


FIG. 2. The Feynman diagram giving rise to the potential of Eq. (5).

¹² L. Fonda and R. G. Newton, *Nuovo Cimento* **14**, 1027 (1959); *Ann. Phys. (N. Y.)* **10**, 490 (1960).

¹³ R. H. Dalitz, *Proc. Roy. Soc. (London)* **A288**, 198 (1965); R. H. Dalitz, T. C. Wong, and G. Rajasekaran, *Phys. Rev.* **153**, 1617 (1967).

and at the PPV vertex the $SU(3)$ invariant interaction is

$$\frac{1}{\sqrt{2}}g_{\rho 0\pi+\pi}V_{\mu j}^i[P_k^j\partial P_i^k/\partial x_\mu - P_i^k\partial P_k^j/\partial x_\mu]. \quad (2)$$

Here B_j^i is the octet tensor of baryon fields, etc. From the theory of nuclear forces one finds

$$g_{pp\rho 0}^2/4\pi \sim 1.2-1.8. \quad (3)$$

From the width of the ρ meson one has

$$g_{\rho 0\pi+\pi}^2/4\pi = 2.0. \quad (4)$$

We evaluate the diagram in Fig. 2 in the static limit, where it reduces to a Yukawa potential. We also assume at this stage perfect $SU(3)$ symmetry, so that the masses of the exchanged vector mesons are all the same and the fourth component of the momentum transfer vanishes. We thus find the potential

$$\begin{aligned} V &= +\frac{G^2 e^{-m_\rho r}}{4\pi r} [B_j^k B_k^i - B_k^i B_j^k] [P_j^l P_l^i - P_l^j P_i^l] \\ &= -\frac{G^2 e^{-m_\rho r}}{4\pi r} [6|1\rangle\langle 1| + 3|8_s\rangle\langle 8_s| \\ &\quad + 3|8_a\rangle\langle 8_a| - 2|27\rangle\langle 27|]. \end{aligned} \quad (5)$$

Here we have

$$\frac{G^2}{4\pi} = \frac{g_{pp\rho 0}g_{\rho 0\pi+\pi}}{4\pi}, \quad (6)$$

and we take m_ρ to be the mass of the ρ meson. The states $|1\rangle$, $|8_s\rangle$, etc., are normalized singlet, symmetric octet, etc., states. We see that the potential is attractive for the singlet state and the two octet states and repulsive for the 27 state. Since isospin $\frac{3}{2}$ occurs only in the 27 state it is clear that the above potential can never account for an S_{31} resonance such as $N_{3/2}^*(1670)$.

With the potential (5) and perfect $SU(3)$ symmetry we could for sufficiently large G produce S -wave bound states in the singlet and octet states, but the Yukawa potential would not produce an S -wave resonance. We shall break the $SU(3)$ symmetry by employing (5) in a Schrödinger equation in which we use the real physical masses for the pseudoscalar mesons and the baryons. In order to do this it is convenient to rewrite the potential (5) as a matrix in channel space,

$$V_{ij}(r) = -\frac{G^2 e^{-m_\rho r}}{4\pi r} C_{ij}. \quad (7)$$

For the various possible choices of isospin and hypercharge we have the following matrices C :

$I = \frac{1}{2}, Y = 1$:

$$C = \begin{matrix} & \pi N & \eta N & K\Lambda & K\Sigma \\ \begin{matrix} \pi N \\ \eta N \\ K\Lambda \\ K\Sigma \end{matrix} & \begin{bmatrix} 2 & 0 & \frac{3}{2} & -\frac{1}{2} \\ 0 & 0 & -\frac{3}{2} & -\frac{3}{2} \\ \frac{3}{2} & -\frac{3}{2} & 0 & 0 \\ -\frac{1}{2} & -\frac{3}{2} & 0 & 2 \end{bmatrix} \end{matrix}. \quad (8)$$

$I=0, Y=0:$

$$C = \begin{matrix} & \pi\Sigma & \bar{K}N & \eta\Lambda & K\Xi \\ \begin{matrix} \pi\Sigma \\ \bar{K}N \\ \eta\Lambda \\ K\Xi \end{matrix} & \begin{bmatrix} 4 & -(\sqrt{6})/2 & 0 & (\sqrt{6})/2 \\ -(\sqrt{6})/2 & 3 & 3\sqrt{2}/2 & 0 \\ 0 & 3\sqrt{2}/2 & 0 & -3\sqrt{2}/2 \\ (\sqrt{6})/2 & 0 & -3\sqrt{2}/2 & 3 \end{bmatrix} \end{matrix} \quad (9)$$

$I=1, Y=0:$

$$C = \begin{matrix} & \pi\Lambda & \pi\Sigma & \bar{K}N & \eta\Sigma & K\Xi \\ \begin{matrix} \pi\Lambda \\ \pi\Sigma \\ \bar{K}N \\ \eta\Sigma \\ K\Xi \end{matrix} & \begin{bmatrix} 0 & 0 & -(\sqrt{6})/2 & 0 & -(\sqrt{6})/2 \\ 0 & 2 & -1 & 0 & 1 \\ -(\sqrt{6})/2 & -1 & 1 & -(\sqrt{6})/2 & 0 \\ 0 & 0 & -(\sqrt{6})/2 & 0 & -(\sqrt{6})/2 \\ -(\sqrt{6})/2 & 1 & 0 & -(\sqrt{6})/2 & 1 \end{bmatrix} \end{matrix} \quad (10)$$

$I=\frac{1}{2}, Y=-1:$

$$C = \begin{matrix} & \pi\Xi & \eta\Xi & \bar{K}\Lambda & \bar{K}\Sigma \\ \begin{matrix} \pi\Xi \\ \eta\Xi \\ \bar{K}\Lambda \\ \bar{K}\Sigma \end{matrix} & \begin{bmatrix} 2 & 0 & \frac{3}{2} & -\frac{1}{2} \\ 0 & 0 & -\frac{3}{2} & -\frac{3}{2} \\ \frac{3}{2} & -\frac{3}{2} & 0 & 0 \\ -\frac{1}{2} & -\frac{3}{2} & 0 & 2 \end{bmatrix} \end{matrix} \quad (11)$$

The matrix potential (7) is employed in a multi-channel Schrödinger equation, which for the radial wave function $U_i(r) = r\psi_i(r)$ for S waves has the form

$$-\frac{1}{2\mu_i} \frac{d^2 U_i(r)}{dr^2} + \sum_j V_{ij}(r) U_j(r) = (E - m_{1i} - m_{2i}) U_i(r). \quad (12)$$

Here E is the total energy, m_{1i} and m_{2i} are the masses of the two particles in channel i , and μ_i is a reduced mass. We have attempted to take some account of relativistic kinematics by using an energy-dependent reduced mass defined as follows:

$$E = (p^2 + m_{1i}^2)^{1/2} + (p^2 + m_{2i}^2)^{1/2} = m_{1i} + m_{2i} + p^2/2\mu_i(E), \quad (13)$$

or equivalently

$$\mu_i(E) = [E^2 - (m_{1i} - m_{2i})^2][E + m_{1i} + m_{2i}]/8E^2. \quad (14)$$

This method was introduced by Rajasekaran.¹⁴ The static approximation used in order to obtain a potential and the energy-dependent reduced mass (14) are crude approximations. They lead to a set of coupled differential equations easily solved on a computer. A more careful treatment of recoil and relativistic kinematics leads to a set of coupled integral equations in momentum space; these are considerably more complicated numerically.

We can superpose the solutions of (12) so as to obtain solutions which outside the range of the potential have the form

$$U_{ji}(r) = F_i(k_i r) \delta_{ji} + G_j(k_j r) K'_{ji}, \quad (15)$$

where k_i is the wave number in channel i and F and G are of the form

$$F_i(k_i r) = \begin{cases} (\mu_i/k_i)^{1/2} \sin k_i r, & k_i^2 > 0, \text{ open channel} \\ 0, & k_i^2 < 0, \text{ closed channel} \end{cases} \quad (16)$$

$$G_i(k_i r) = \begin{cases} (\mu_i/k_i)^{1/2} \cos k_i r, & k_i^2 > 0, \text{ open channel} \\ e^{-\kappa_i r}, & \kappa_i = +\sqrt{(-k_i^2)}, \\ & k_i^2 < 0, \text{ closed channel.} \end{cases} \quad (17)$$

In (15) there is a standing wave $\sin k_i r$ in the open channel i and standing waves $\cos k_j r$ in all open channels j . In the closed channels we have exponentially decaying wave functions. From the numerical solution of Eq. (12) we obtain the matrix K'_{ji} of (15). If some of the channels are closed, we discard the matrix elements referring to closed channels and are left with a square matrix K'_{ji} referring to open channels.

This matrix, which is real and symmetric, is the reduced K' matrix discussed for example by Dalitz.¹⁵ It has eigenvalues $\tan \delta_\alpha$ and normalized eigenvectors $v_{i\alpha}$. The δ_α are then the eigenphases, the multichannel generalization of phase shifts. The T' matrix, which is the T matrix with a kinematic factor removed is then

$$T'_{ji} = \left(\frac{K'}{1 - iK'} \right)_{ji} = \sum_\alpha v_{i\alpha} v_{j\alpha} e^{i\delta_\alpha} \sin \delta_\alpha, \quad (18)$$

and from this we obtain the S -wave cross sections

$$\sigma_{ji} = (4\pi/k_i^2) |T'_{ji}|^2, \quad (19)$$

where i refers to the initial and j to the final state.

For a four-channel problem it takes about 6 sec to perform all these calculations at one energy on an IBM 7094 computer.

II. RESULTS OF CALCULATIONS

We present in this section the results of the numerical calculations for the model discussed above. Although the model is too crude to expect a close fit to experimental data, we shall find that a very rough qualitative agreement can be achieved for a suitable choice of the coupling constant $G^2/4\pi$, which is the only parameter we have varied in these calculations.

We present our results in the form of several kinds of graphs. First we have Argand diagrams such as Fig. 1 of the real versus the imaginary parts of the scattering amplitude

$$2kf = 2e^{i\delta} \sin \delta = 2T'_{ii} \quad (20)$$

as a function of energy. Here $\delta = \delta_r + i\delta_i$ is the complex phase shift in some specified channel, and we note that $2kf$ is twice a diagonal element of the T' matrix (18). We recall the geometrical significance of such a diagram in Fig. 3. Unitarity limits $2kf$ to the interior of a circle of unit radius about the point i . If only one channel is open so that the scattering is elastic, $2kf$ lies on the

¹⁴ G. Rajasekaran, Nuovo Cimento **37**, 1004 (1965).

¹⁵ R. H. Dalitz, Ann. Rev. Nucl. Sci. **13**, 350 (1963).

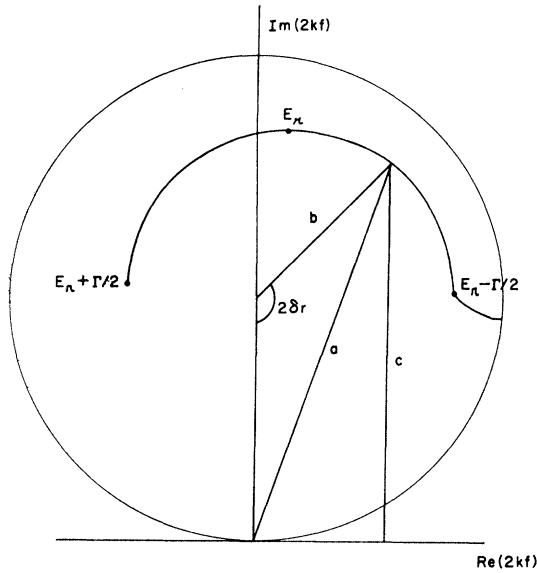


FIG. 3. An example of an Argand diagram for the scattering amplitude. The significance of the curve is given by Eqs. (20) and (21).

unit circle; if two or more channels are open so that the scattering is inelastic, $2kf$ lies inside the unit circle. The scattering cross section σ_s , the reaction cross section σ_r , and the total cross section σ_t are given by

$$\begin{aligned}\sigma_s &= (\pi/k^2) |a|^2, \\ \sigma_r &= (\pi/k^2) (1 - |b|^2), \\ \sigma_t &= (2\pi/k^2) |c|^2,\end{aligned}\quad (21)$$

with a, b, c as indicated in Fig. 3.

We also note that for multichannel S -wave scattering there is a cusp in the Argand diagrams of $2kf$ at the threshold of each channel; in fact the curve of $\text{Re}2kf$ versus $\text{Im}2kf$ as a function of energy makes a 90° left-hand turn. This happens because near the threshold f is a linear function ($f = a + bq$) of the momentum in the opening channel. Above the threshold q is real; below the threshold, $q = i|q|$ is positive imaginary, so that the outgoing wave $\exp(iqr)$ becomes a decaying exponential. These cusps are clearly indicated in the results given below.

There are various ways of defining a resonance. Of course for a single-channel problem we have the condition that the (real) phase shift increases through 90° . This corresponds to the amplitude $2kf$ traversing the top of the unitarity circle in Fig. 3 in a counterclockwise direction. On the other hand, even for a multichannel problem, if a resonance can be represented by a Breit-Wigner term plus a constant complex background term, the Argand diagram of $2kf$ will be semicircular in a counterclockwise sense as indicated in the example of Fig. 3. The energy at the top of the circle is the resonance energy E_r ; the energies at the edges of the semi-circle are $E_r \pm \Gamma/2$, where Γ is the width of the resonance.

Another possible condition for a resonance in a multi-channel system is that one of the (necessarily real) eigenphases δ_α goes through 90° . The resonance energy E_r would then be the energy at which this occurs. We give some results for the eigenphases below, and it will be seen that these two definitions of E_r lead in general to somewhat different results. The experimentalists generally give the resonance energy as the energy of the peak in an appropriate mass distribution. A related, although somewhat shifted peak would be obtained in a scattering cross section, for which we also give some numerical results below.

A. $I = \frac{1}{2}, Y = 1$ State

In Fig. 4 we give the Argand diagram of the amplitude (20) for the πN channel in the $I = \frac{1}{2}$ state for the particular choice of coupling constant $G^2/4\pi = 0.91$. The curve in Fig. 4 is qualitatively similar to the experimental curve in Fig. 1, but obviously there is no quantitative agreement. If the coupling constant $G^2/4\pi$ is reduced from the value 0.91, the point at which the curve in Fig. 5 leaves the unitarity circle (the ηN threshold) moves down the side of the unitarity circle and the size of the loop associated with the ηN threshold rapidly diminishes; at $G^2/4\pi = 0.85$ the loop has completely disappeared. If the coupling constant is increased, the point where the curve leaves the unitarity circle moves up the side of the unitarity circle and the loop associated with the ηN threshold rapidly expands; at $G^2/4\pi = 0.93$ this loop fills the whole unitarity circle. Thus for $G^2/4\pi = 0.91$ there is a resonance slightly above the ηN threshold, and for $G^2/4\pi = 0.93$ there is a resonance

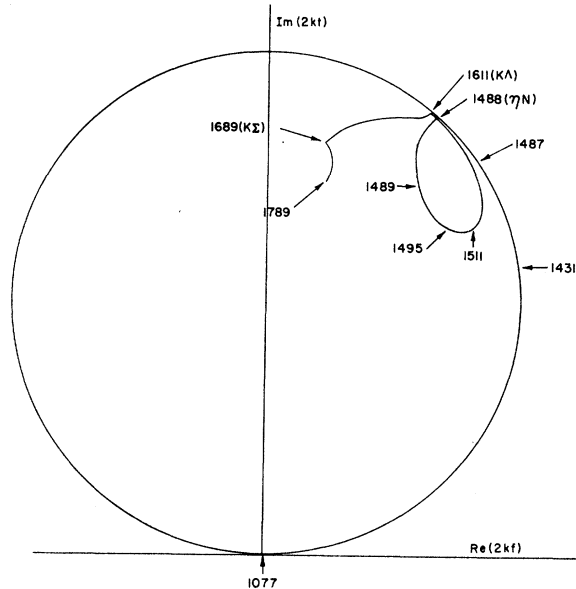


FIG. 4. The Argand diagram for πN scattering in the $I = \frac{1}{2}$, $Y = +1$ state for the coupling constant $G^2/4\pi = 0.91$. The numbers give energies in MeV. Thresholds are indicated by particle symbols in parentheses.

slightly below the ηN threshold. This latter case is similar to the $Y_0^*(1405)$, which we consider below. In Fig. 5 we give the cross sections for $G^2/4\pi=0.91$. In Fig. 6 the solid curves are the eigenphases for $G^2/4\pi=0.91$. It will be noted that one of the eigenphases goes through 90° at 1501 MeV, which corresponds to the bottom of the loop in Fig. 4.

It is rather remarkable that one obtains this resonance associated with the ηN threshold at all with the potential (7), (8) since the πN and ηN channels are not directly coupled with each other; the only coupling comes through the higher-mass closed channels $K\Lambda$ and $K\Sigma$. (In fact it is easy to verify from conservation of G parity and isospin that exchange of a vector meson cannot transform a π meson into an η meson. The simplest exchange which would achieve this is A_2 exchange.) The absence of direct coupling presumably accounts for the extreme narrowness of the calculated resonance of Fig. 5 compared to the experimental resonance of Fig. 1. In order to obtain a more realistic model we would have to include exchange of the 2^+ nonet and also the BV channels.

In an attempt to understand the origin of the resonance associated with the ηN threshold we have carried out some auxiliary calculations, which are recorded in Fig. 6. The dashed curves give the eigenphases when the πN channel is almost decoupled. To obtain the dashed curves we made the following replacements in the matrix (8): $C_{13}=C_{31}\rightarrow 0.15$, $C_{14}=C_{41}\rightarrow -0.05$. If

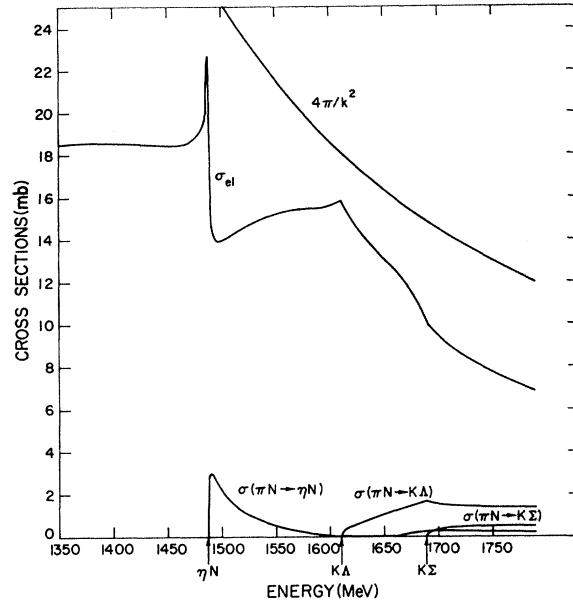


FIG. 5. The cross sections for elastic- πN scattering and for $\pi N \rightarrow \eta N$, $\pi N \rightarrow K\Lambda$, $\pi N \rightarrow K\Sigma$ in the $I=\frac{1}{2}$ state for $G^2/4\pi=0.91$.

these elements of the matrix C are taken to be zero, the eigenphases are essentially identical to the dashed curves, except that the two curves now cross at 1489 MeV. The nearly horizontal sections give the decoupled

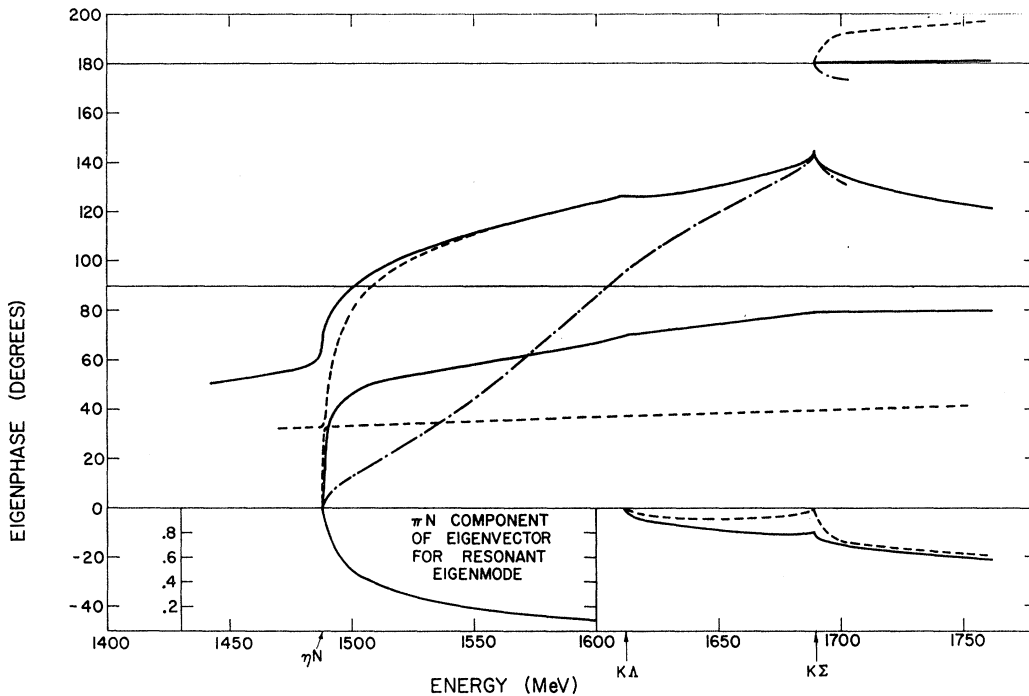


FIG. 6. Eigenphases for the $I=\frac{1}{2}$, $Y=+1$ state. The solid curves give the eigenphases for $G^2/4\pi=0.91$. The dashed curves give the eigenphases for $G^2/4\pi=0.91$ and the $\pi N-K\Lambda$ and $\pi N-K\Sigma$ couplings in the matrix (8) reduced by a factor of 10. The dot-dash curves give the eigenphases for $G^2/4\pi=0.91$ for the two-channel problem with the coupling matrix (22). The insert at the bottom of the figure gives the πN component of the eigenvector corresponding to the eigenphase which goes through 90° at 1501 MeV.

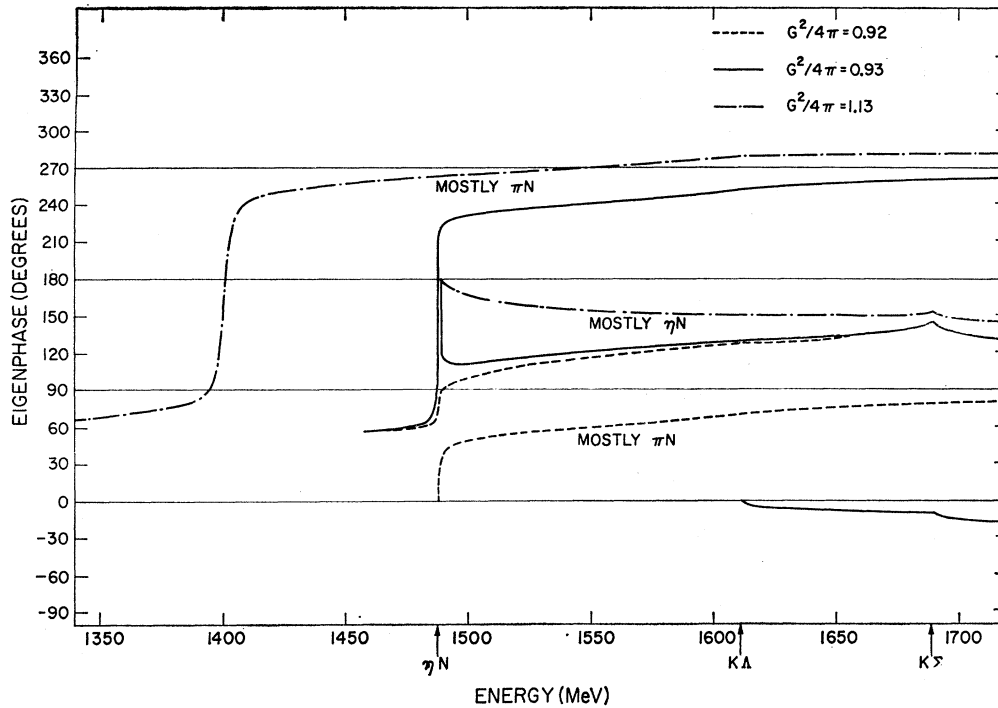


FIG. 7. Eigenphases for the $I=\frac{1}{2}$, $Y=+1$ state with three different choices of coupling constant.

πN phase shift of about 35° . It is seen that the resonance persists even when the πN channel is decoupled. The broken curve in Fig. 6 gives the eigenphase when both the πN and $K\Lambda$ channels are decoupled. Thus the broken curve is for a two-channel problem with a C matrix

$$\begin{pmatrix} \eta N & K\Sigma \\ 0 & -\frac{3}{2} \end{pmatrix} \quad (22)$$

$$K\Sigma \begin{pmatrix} -\frac{3}{2} & 2 \end{pmatrix}.$$

We see from Fig. 6 that there is still a resonance although it has now moved to somewhat higher energies. The resonance is now a virtual bound state of $K\Sigma$ which can decay through the ηN channel. To the extent that it is possible to give a simple description of the origin of the resonance in this model involving four-coupled channels it would seem that it is basically a bound state of $K\Sigma$.¹⁶

In Fig. 7 we give some results for larger values of the coupling constant $G^2/4\pi$. These show what happens to the eigenphases as the resonance moves below the ηN threshold. Although these curves do not correspond to the actual physical situation, it seems worthwhile to record some examples of the behavior of eigenphases under various conditions. At $G^2/4\pi=0.92$ the resonance is still above the threshold. At $G^2/4\pi=0.93$ it has moved below the threshold. When the resonance energy

¹⁶ For the $K\Sigma$ channel alone the well-depth parameter [J. M. Blatt and V. F. Weisskopf, *Theoretical Nuclear Physics* (John Wiley & Sons, Inc., New York, 1952), p. 56] is given by $S=0.595$ ($2\mu/m_0$) ($2G^2/4\pi$) = 0.985 for $G^2/4\pi=0.91$, so that without any coupling to other channels the $K\Sigma$ system just misses having a bound state.

(defined as the energy at which the eigenphase goes through 90°) crosses the threshold energy there is a discontinuous jump in the eigenphases. When the resonance is above threshold, one of the eigenphases starts at 0° . If the resonance is below threshold, one of the eigenphases starts from 180° . In order to "get out of the way" the other eigenphase is pushed up above 180° . (In this region the K' matrix is a real, symmetric 2×2 matrix. If such a matrix is to have two identical eigenvalues it must be a multiple of the unit matrix. Ruling out such an exceptional possibility, the eigenphase curves cannot cross.) Note, however, that the dashed curve below 90° for $G^2/4\pi=0.92$ is essentially identical to the solid curve above 180° for $G^2/4\pi=0.93$. Thus this section of the eigenphase curve is displaced upward by 180° when the resonance crosses threshold. We note that the behavior of the eigenphases when the resonance is near threshold is different for this case from the case of the $Y_0^*(1405)$ discussed below. Presumably the difference has to do with the fact that for the present case the resonance is due to a bound state in a higher-mass channel ($K\Sigma$). In the insert at the bottom of Fig. 6 we have plotted the πN component of the normalized eigenvector associated with the eigenphase which goes through 90° above the ηN threshold. This eigenvector is pure πN below the ηN threshold; above the threshold the πN component drops rapidly and this eigenvector soon becomes mostly ηN . In the other graphs of eigenphases we have simply indicated the principal component of the eigenvectors by statements like "mostly ηN ."

Returning to Fig. 4, we see that above the loop

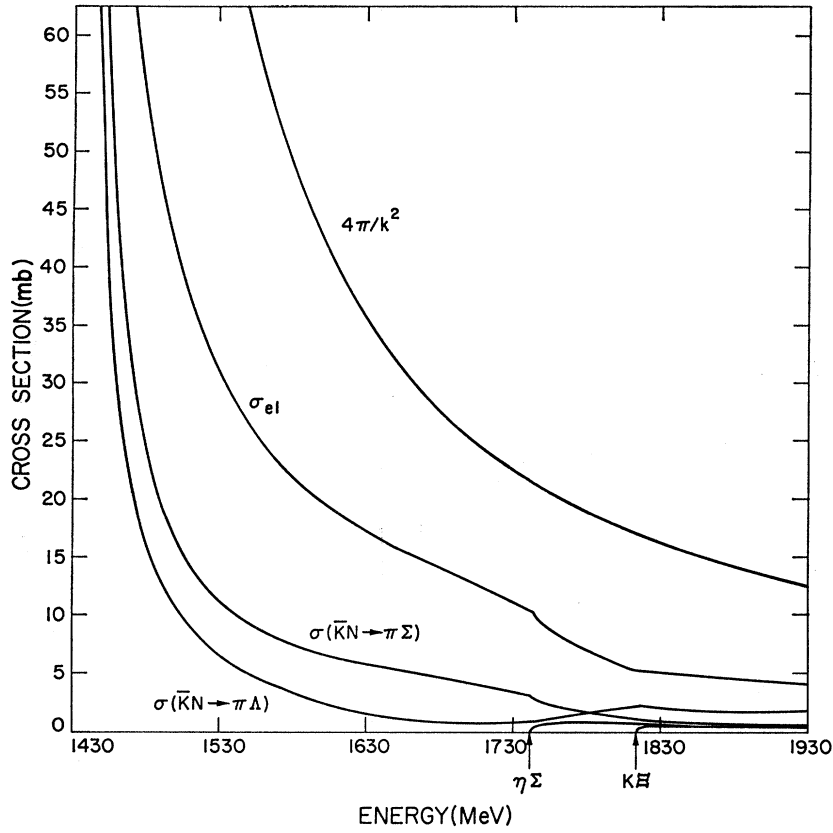


FIG. 9. The cross sections for elastic- $\bar{K}N$ scattering and for $\bar{K}N \rightarrow \pi\Lambda$, $\bar{K}N \rightarrow \pi\Sigma$, $\bar{K}N \rightarrow \eta\Sigma$, $\bar{K}N \rightarrow K\Xi$ in the $I=1$ state for $G^2/4\pi=0.91$.

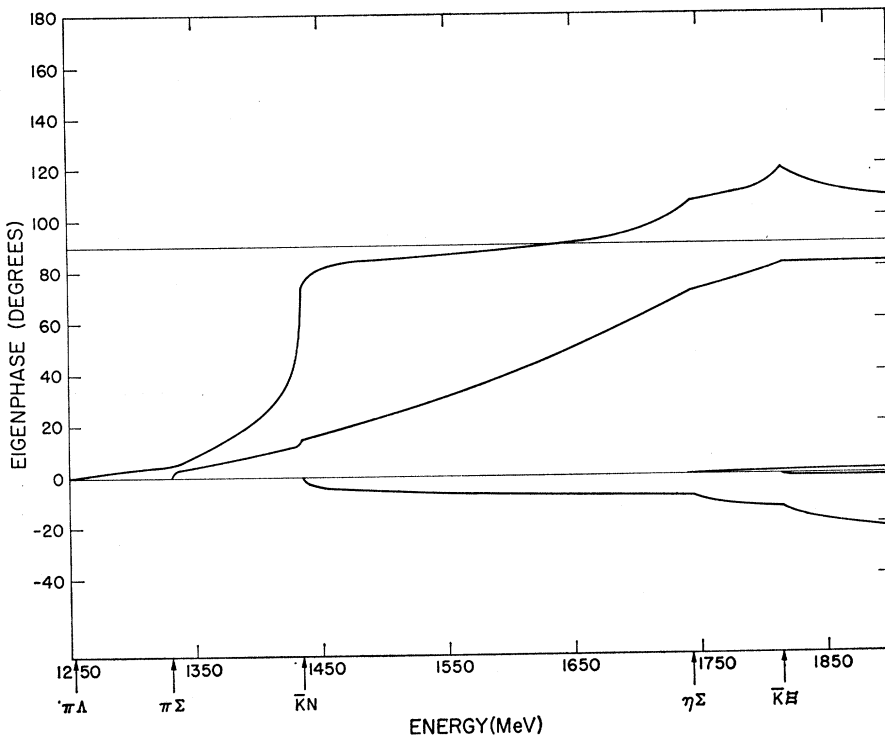
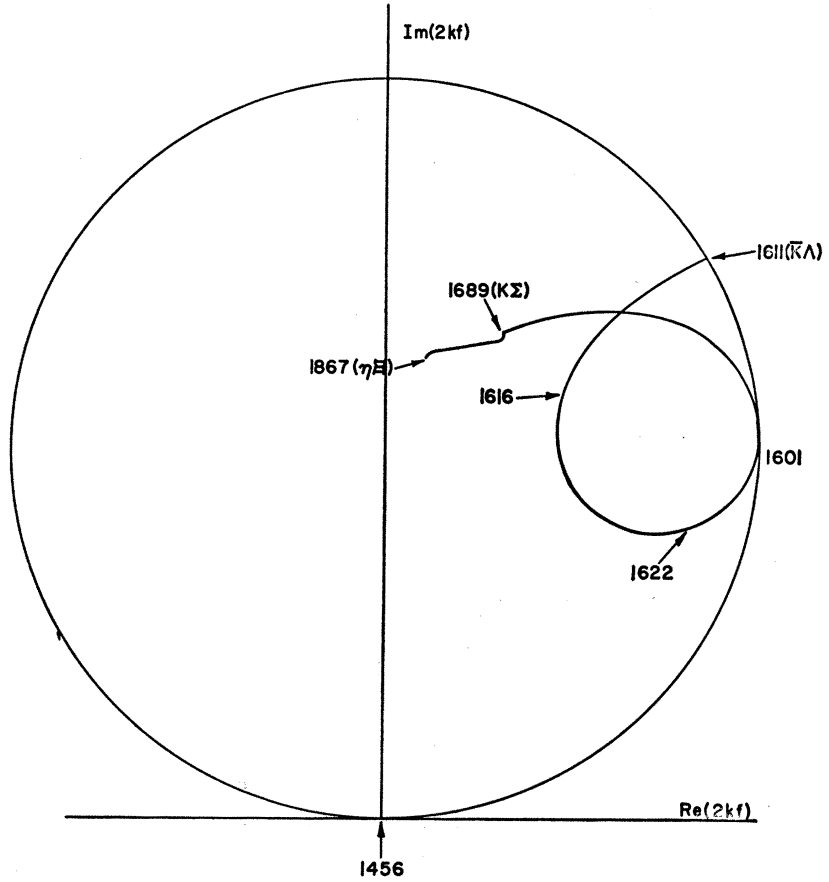


FIG. 10. Eigenphases for the $I=1, Y=0$ state for $G^2/4\pi=0.91$.

FIG. 11. The Argand diagram for $\pi\Xi$ scattering in the $I=\frac{1}{2}$, $Y=-1$ state for the coupling constant $G^2/4\pi=0.91$. The numbers give energies in MeV. Thresholds are indicated by particle symbols in parentheses.



very slowly, and probably one should not call this a resonance.

C. $I=\frac{1}{2}$, $Y=-1$ State

The results for the $I=\frac{1}{2}$, $Y=-1$ state are given in Figs. 11-13 for $G^2/4\pi=0.91$. As we see from Eqs. (8) and (11) the $SU(3)$ coefficients are the same for this case and for the state $I=\frac{1}{2}$, $Y=+1$ with the particle interchanges $N \rightarrow \Xi$, $K \rightarrow \bar{K}$. Thus the differences between Figs. 4-6 on the one hand and Figs. 11-13 on the other hand are due to the difference between the N and Ξ masses. From examination of Figs. 11-13 we see that our model predicts a $\frac{1}{2}\Xi^*$ resonance at about 1615 MeV. This resonance is essentially a bound state of $\bar{K}\Sigma$, just as the resonance in the $I=\frac{1}{2}$, $Y=+1$ state was a bound state of $K\Sigma$. Note, however, that the resonance appears just above the $\bar{K}\Lambda$ threshold. The $\eta\Xi$ threshold, which is the analog of the ηN threshold for the $I=\frac{1}{2}$, $Y=+1$ state, is now 178 MeV above the $\bar{K}\Sigma$ threshold. In Fig. 14 we give the eigenphases for some larger values of the coupling constant $G^2/4\pi$. The results here are similar to those given in Fig. 7 for the $I=\frac{1}{2}$, $Y=+1$ state. For this case physical reality might correspond to a larger coupling constant for which the resonance lies below the $\bar{K}\Lambda$ threshold.

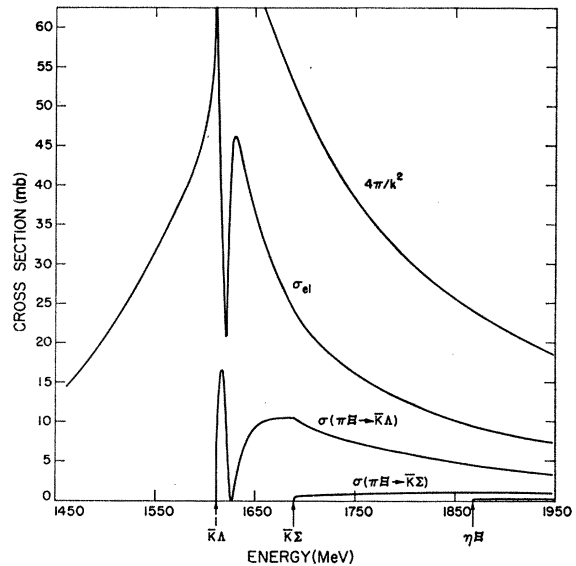


FIG. 12. The cross sections for elastic $\pi\Xi$ scattering and for $\pi\Xi \rightarrow \bar{K}\Lambda$, $\pi\Xi \rightarrow \bar{K}\Sigma$, $\pi\Xi \rightarrow \eta\Xi$ in the $I=\frac{1}{2}$ state for $G^2/4\pi=0.91$.

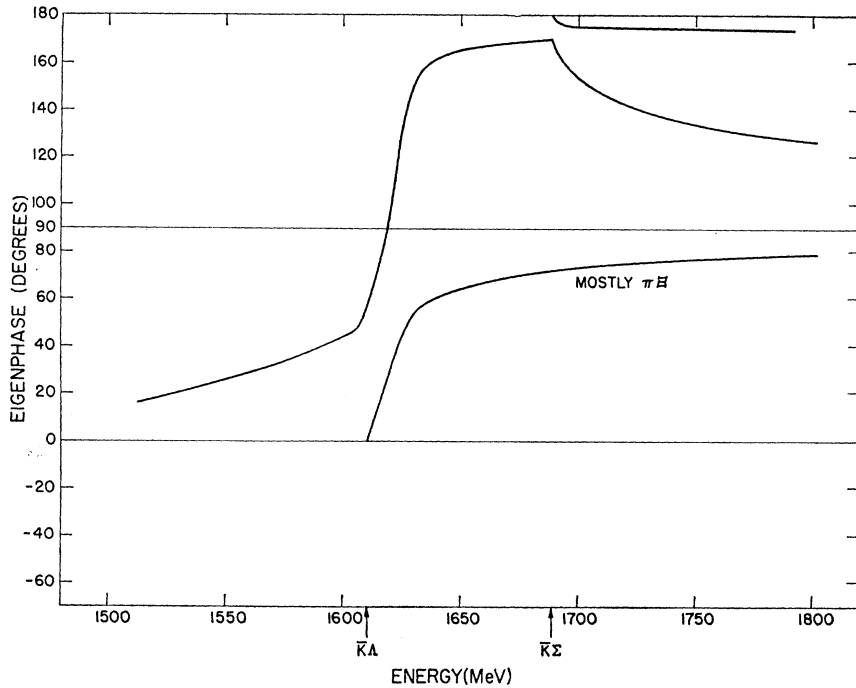


FIG. 13. Eigenphases for the $I = \frac{3}{2}, Y = -1$ state for $G^2/4\pi = 0.91$.

D. $I=0, Y=0$ State

The dominant feature of this state is the existence of the $Y_0^*(1405)$ resonance, which is thought to be a virtual bound state of $\bar{K}N$ which decays through the $\pi\Sigma$ channel.⁷ In order to simplify the problem somewhat we first consider a calculation involving only these two channels. We use for a C matrix the first two rows and columns of (9). The eigenphases and Argand diagrams for this two-channel problem are given for several values of the coupling constant in Fig. 15. We see from Fig. 15

that the coupling constant $G^2/4\pi = 0.91$ used for the other states is too large; it leads to a true bound state (energy below the $\pi\Sigma$ threshold). This is presumably due to the fact that only for the $I=0, Y=0$ state does the strongly attractive $SU(3)$ singlet enter [Eq. (5)]. For the two-channel problem a coupling constant of $G^2/4\pi = 0.68$ leads to an eigenphase which goes through 90° at 1413 MeV. The corresponding $\pi\Sigma$ cross section, given in Fig. 16, has a peak at 1408 MeV. The singlet scattering amplitude for the $\bar{K}N$ channel turns out to

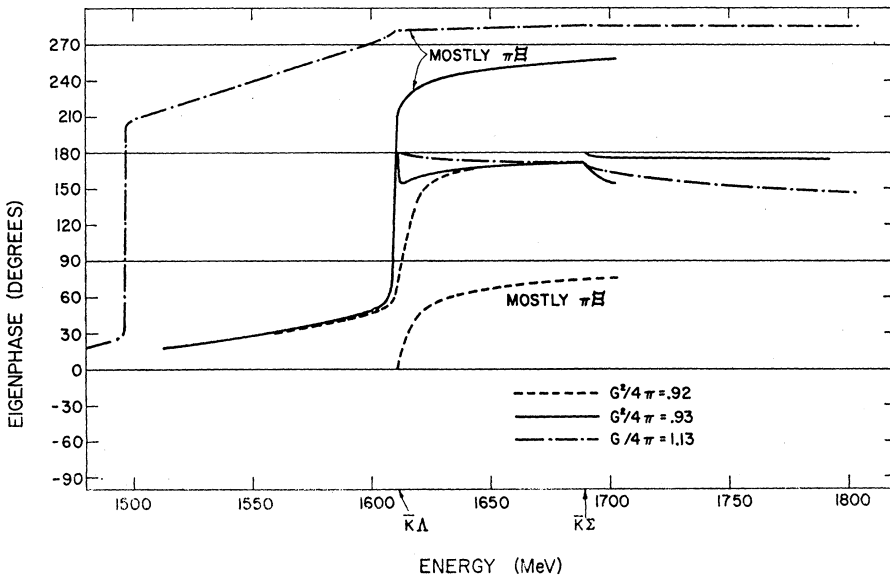


FIG. 14. Eigenphases for the $I = \frac{3}{2}, Y = -1$ state with three different choices of coupling constant.

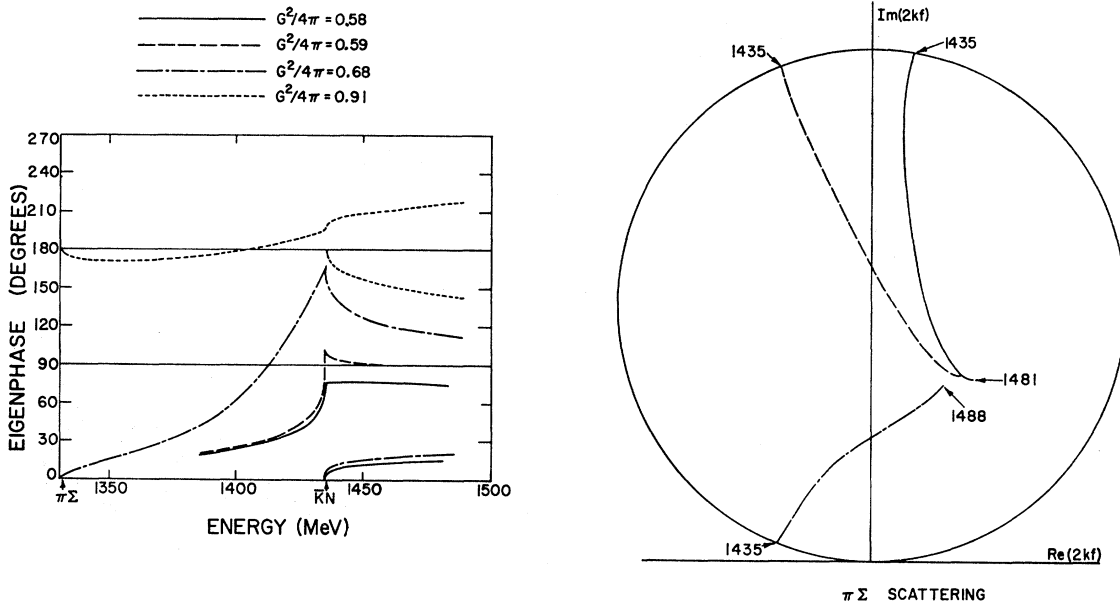


FIG. 15. On the left are plotted the eigenphases for the $I=0, Y=0$ state with just two coupled channels, $\pi\Sigma, \bar{K}N$. On the right are plotted Argand diagrams for $\pi\Sigma$ scattering in the $I=0, Y=0$ state. The curves leave the unitarity circle at the $\bar{K}N$ threshold, 1435 MeV.

be $A_0 = (-1.49 + 0.97i)$ F, which is to be compared with the experimental value given in Eq. (23).

In addition we give in Fig. 15 some results for smaller values of the coupling constant such that the resonance is in the neighborhood of the $\bar{K}N$ threshold. The behavior here is quite different from that discussed in connection with $I=\frac{1}{2}, Y=+1$ state in Sec. 2a. In particular there seems to be no possibility of obtaining a resonance above threshold in the two-channel problem. If the coupling constant is decreased so as to push the resonance above threshold, then the eigenphase no longer goes through 90° . To obtain a resonance above threshold as in Sec. II.A, it seems to be necessary to have a bound state in a higher-mass coupled channel. Another difference between the two- and the four-channel problems has to do with the discontinuous jump in the eigenphases. In the four-channel problem of Sec. II.A this jump occurs when the resonance crosses the threshold. For the two-channel problem (Fig. 15) there is a cusp in one of the eigenphases at the threshold. As the coupling constant is increased, this cusp moves up. When it reaches 180° there is a discontinuous jump in the eigenphases. For the problem represented in Fig. 15 this occurs for a coupling constant of about $G^2/4\pi = 0.74$ (not shown in Fig. 15); for this value of the coupling constant the eigenphase crosses 90° at 1382 MeV.

In Figs. 17–20 we give the numerical results for the four-channel problem in the $I=0, Y=0$ state with the full 4×4 matrix of Eq. (9). We give results for two values of the coupling constant, $G^2/4\pi = 0.56$ and $G^2/4\pi = 0.91$. The smaller value of the coupling constant accounts in a reasonable way for the $Y_0^*(1405)$.

The eigenphase goes through 90° at 1409 MeV and the singlet $\bar{K}N$ scattering length turns out to be $A_0 = (-1.41 + 0.51i)$ F, which is to be compared with

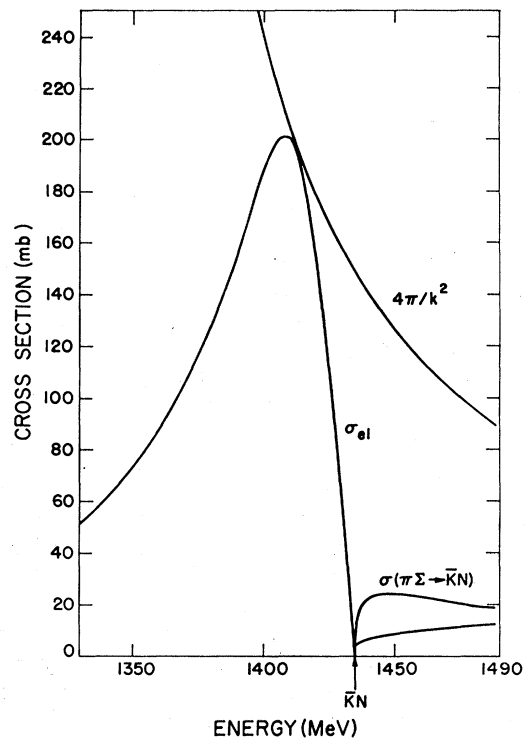


FIG. 16. The cross sections for elastic $\pi\Sigma$ scattering and for the reaction $\pi\Sigma \rightarrow \bar{K}N$ in the $I=0$ state for the problem with just two coupled channels, $\pi\Sigma, \bar{K}N$. $G^2/4\pi = 0.68$.

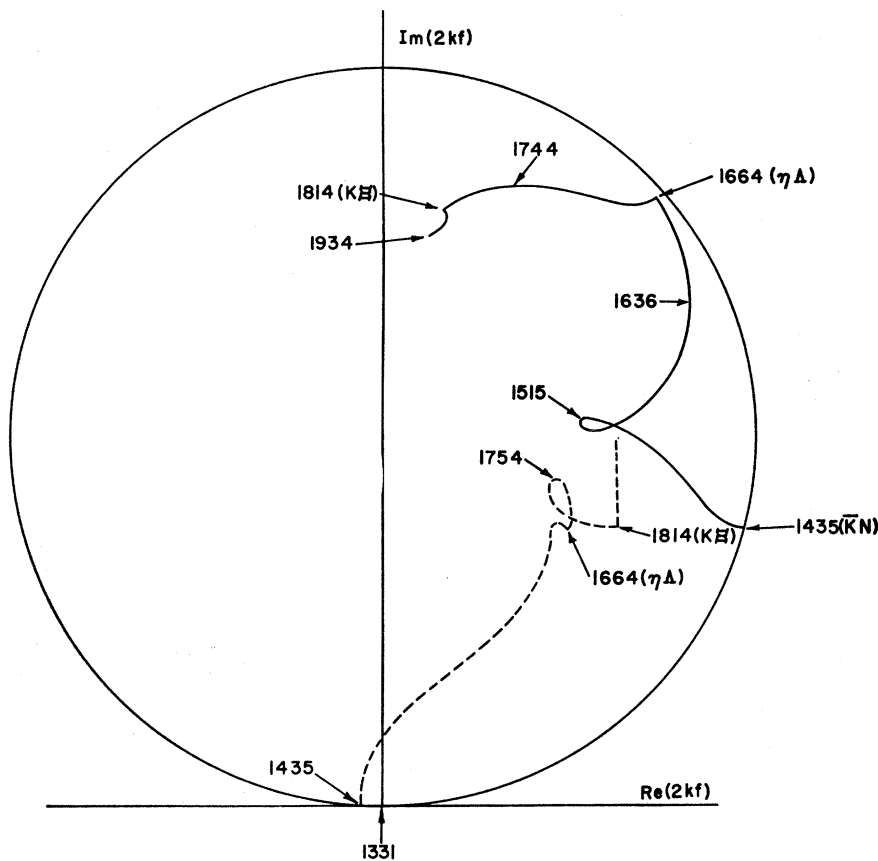


FIG. 17. The Argand diagrams for $\pi\Sigma$ scattering in the $I=0, Y=0$ state for two different values of the coupling constant (solid curve, $G^2/4\pi=0.91$; dashed curve, $G^2/4\pi=0.56$). The numbers give energies in MeV. Thresholds are indicated by particle symbols in parentheses.

the experimental value given in Eq. (23). For the larger value of the coupling constant this resonance has moved below the $\pi\Sigma$ threshold to become a bound state. Correspondingly the phase shift in Fig. 20 starts from 180° at the $\pi\Sigma$ threshold.

On the basis of qualitative considerations one would expect to find another resonance in addition to the $Y_0^*(1405)$ in the $I=0, Y=0$ state. There is a large diagonal element in the $K\Xi$ channel in Eq. (9) and we would thus expect a bound state in the $K\Xi$ channel to yield a resonance just as a bound state in the $K\Sigma$ channel led to a resonance in the $I=\frac{1}{2}, Y=+1$ state. For the smaller coupling constant $G^2/4\pi=0.56$ this does not happen; there are no further resonances in Fig. 20 in addition to the one identified with $Y_0^*(1405)$. For the larger coupling constant $G^2/4\pi=0.91$ there is an additional resonance. One of the eigenphases goes through 270° at 1630 MeV and there are corresponding indications of resonance in the Argand diagram of Fig. 18 and the elastic-cross-section curve in Fig. 19.

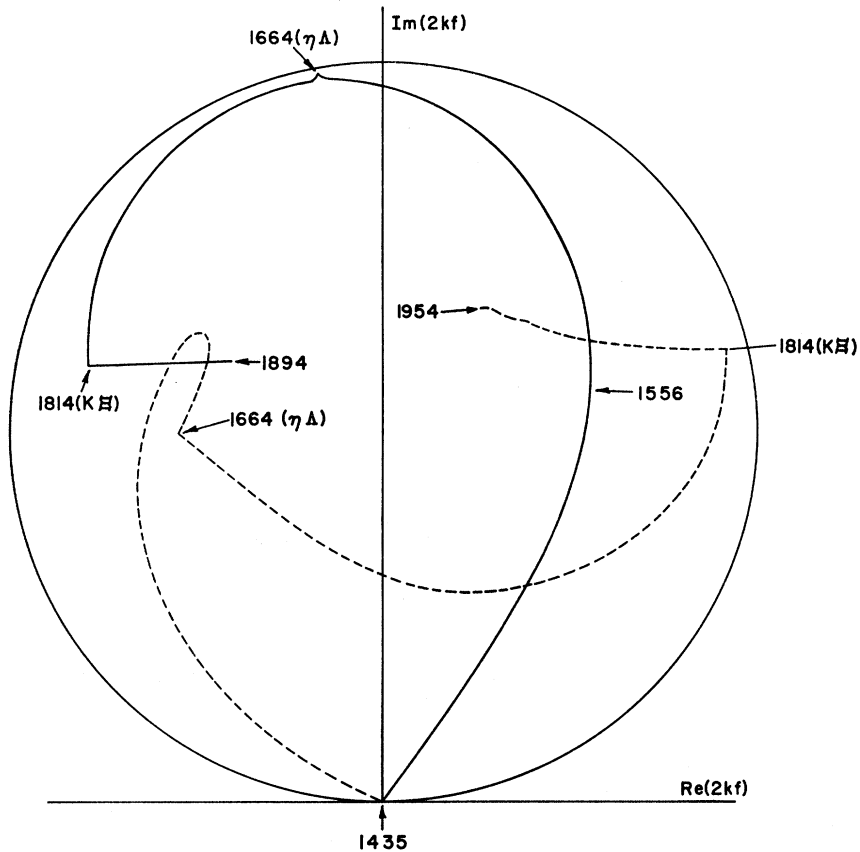
There is experimental evidence for a resonance with these quantum numbers in the work of Berley *et al.*⁸ These workers discovered the resonance in the reaction $\bar{K}N \rightarrow \eta\Delta$, where it causes a sharp rise and fall in the cross section $\sigma(\bar{K}N \rightarrow \eta\Delta)$ near threshold with a peak value of about 1.0 mb. We do not find such a sharp rise and fall in the cross section as calculated in the model

studied in this paper; instead there is a gradual rise to a value of about 0.4 mb. For the coupling constant $G^2/4\pi=0.91$ the calculated resonance lies at 1630 MeV according to Fig. 20. This is 34 MeV below the $\eta\Delta$ threshold. By decreasing the coupling constant we can move the resonance above the threshold. For a coupling constant $G^2/4\pi=0.88$ the eigenphase goes through 90° at 1677 MeV, which is 13 MeV above the $\eta\Delta$ threshold and close to the value given for the resonance energy by Berley *et al.*⁹ Otherwise the eigenphase curves are very similar to those shown in Fig. 20 for $G^2/4\pi=0.91$. The cross section $\sigma(\bar{K}N \rightarrow \eta\Delta)$ is almost the same for the two cases $G^2/4\pi=0.88$ and $G^2/4\pi=0.91$. There is no sharp rise and fall of the cross section such as is found experimentally and in our model calculation for $\sigma(\pi N \rightarrow \eta N)$.

III. CONCLUSIONS

We have studied a simple model for the S -wave scattering of the pseudoscalar-meson octet by the baryon octet. The actual physical masses of the particles are used, so that the $SU(3)$ symmetry is broken and the problem becomes one involving coupled channels. By making drastic approximations in the kinematics and the potential we obtain a problem which in

FIG. 18. The Argand diagrams for $\bar{K}N$ scattering in the $I=0, Y=0$ state for two different values of the coupling constant (solid curve, $G^2/4\pi = 0.91$; dashed curve, $G^2/4\pi = 0.56$). The numbers give energies in MeV. Thresholds are indicated by particle symbols in parentheses.



a reasonably convenient way is exactly soluble, albeit numerically.

We find that it is relatively easy to produce S -wave resonances in this coupled-channel model with only Yukawa potentials. These resonances are more or less complex examples of virtual bound states of the type discussed by Dalitz and Tuan⁷—a bound state in a higher-mass channel gives rise to a resonance in a coupled lower-mass channel. In the example discussed in the first part of Sec. II.D there are only two coupled channels; the bound state in the higher-mass channel gives rise to the resonance in the lower-mass channel. In this example the resonance can only appear below the threshold of the higher-mass channel. In the example of Sec. II.A there are four coupled channels— πN , ηN , $K\Lambda$, $K\Sigma$ in order of increasing mass. The resonance seems to be due to a bound state in the highest mass channel, $K\Sigma$. For the interesting choice of the coupling constant near the ηN threshold and by varying the coupling constant can be made to appear above or below the threshold.

The model is so crude that we can hardly expect a good fit to the experimental data. In addition to all the kinematic simplifications, we have considered only vector-meson exchange and have included only the channels involving one pseudoscalar meson and one

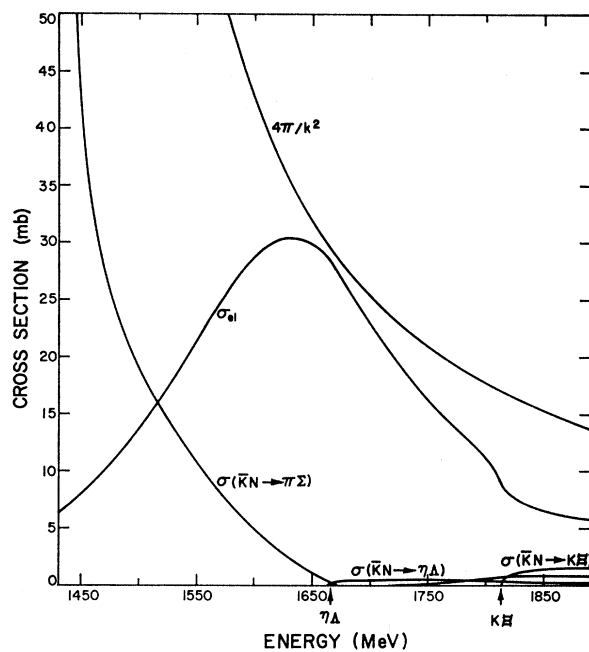


FIG. 19. The cross sections for elastic $\bar{K}N$ scattering and for the reactions $\bar{K}N \rightarrow \pi\Sigma$, $\bar{K}N \rightarrow \eta\Lambda$, $\bar{K}N \rightarrow K\Sigma$ in the $I=0$ state for $G^2/4\pi = 0.91$.

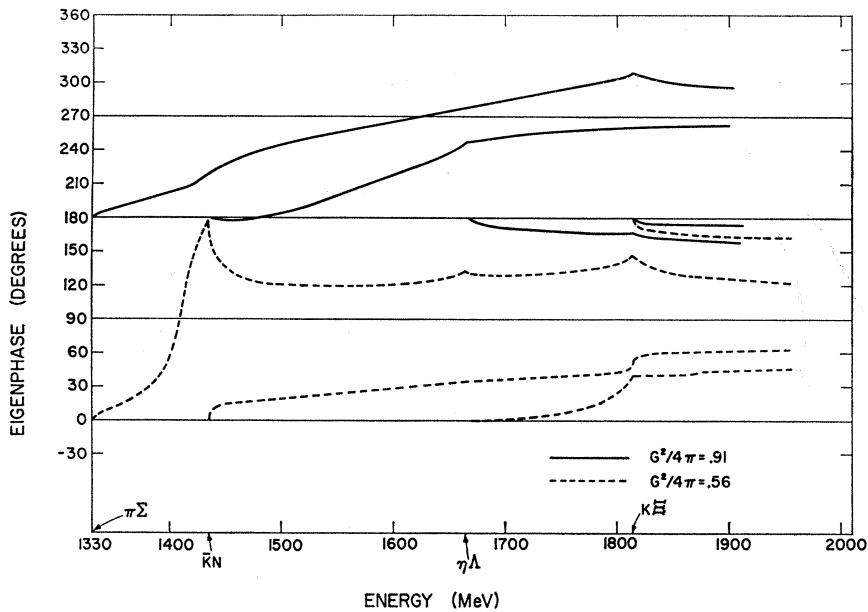


FIG. 20. Eigenphases for the $I=0$, $Y=0$ state for two different choices of coupling constant.

baryon. Clearly there are important corrections due to baryon exchange, $(\pi\pi)$ exchange, 2^+ octet exchange and other coupled channels such as baryon-vector-meson and three-body channels. Nonetheless there is a strong qualitative similarity between the predictions of the model and experimental fact. As we have seen in Sec. II.D it is quite easy to account for the $Y_0^*(1405)$. In Sec. II.A we seem to have produced a theory of the $N_{1/2}^*(1570)$ in which it is to be qualitatively understood as a bound state in the $K\Sigma$ channel. We also find a resonance in the $I=0$, $Y=0$ state close to the $\eta\Lambda$ threshold, although the calculated cross section $\sigma(KN \rightarrow \eta\Lambda)$ does not have the sharply peaked character found experimentally and associated with the $Y_0^*(1670)$.⁹

Finally the model predicts a Ξ^* resonance at about 1615 MeV. The model does not yield a resonance in the $I=1$, $Y=0$ state. Although one of the eigenphases goes through 90° in this state, it goes through so slowly that there are no bumps in the cross sections. In a model in which the $SU(3)$ symmetry is so badly broken we should not be surprised if there are some missing members in the $SU(3)$ multiplets.

ACKNOWLEDGMENTS

The author is indebted to his colleagues, particularly J. D. Jackson and R. L. Schult, for valuable discussions and suggestions.